Narrowband Thermal Emission Realized through the Coupling of Cavity and Tamm Plasmon Resonances

Zhiyu Wang, J. Kenji Clark, Ya-Lun Ho, Bertrand Vilquin, Hirofumi Daiguji, Jean-Jacques Delaunay

ACS Photonics

Article

Cite This: ACS Photonics XXXX, XXX, XXX−XXX

Narrowband Thermal Emission Realized through the Coupling of Cavity and Tamm Plasmon Resonances

Zhiyu Wang,[†] J. Kenji Clark,[†] Ya-Lun Ho,[†] Bertrand Vilquin,[‡] Hirofumi Daiguji,[†] and Jean-Jacques Delaunay*[,†]

[†]Department of Mechanical Engineering, School of Engineering, The University of Tokyo, Tokyo 113-8656, Japan

[‡]Université de Lyon, École centrale de Lyon, Institut des nanotechnologies de Lyon, 36 avenue Guy de Collongue, 69130 Ecully, France

Supporting Information

ABSTRACT: A hybrid structure that supports the coupling of a cavity mode and a Tamm plasmon (TP) mode is demonstrated as a spectrally selective thermal emitter for the mid-infrared spectral range. Unlike conventional TP structures, the presented hybrid structure contains an optical cavity sandwiched between the distributed Bragg reflector (DBR) and the metallic mirror of a typical TP structure. In simulation, the TP-cavity hybrid structure exhibits a strong peak (absorptance = 0.993) in the absorption spectrum with a high quality factor (Q = 135), and this absorptance peak can exist over a wide range of resonance wavelengths by adjusting the cavity thickness. Moreover, the hybrid structure shows a small polarization dependence (for incident angles less than 30°, the resonance wavelength of TM and TE differ by less than 2 nm) and a shift of less than 20 nm in the absorptance peak wavelength for incident angles between 0° and 8°. The absorptance peak of the hybrid structure is stronger and sharper than that of a pure TP structure made from the same materials, which has a maximum absorptance of 0.898 and Q-factor of 28, and a Fabry−Perot cavity structure topped with a 5 nm Au layer, which has a maximum absorptance of 0.899 and Q-factor of 25. Upon heating, a strong and narrow bandwidth thermal emittance peak is observed with a maximum emittance value of 0.90 and a Q-factor of 88 at a wavelength of 4.731 μm. This easy-to-fabricate and high-performance infrared thermal emitter is ideal for applications where narrowband infrared light sources are required.

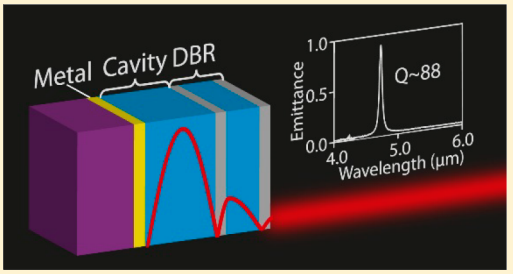

KEYWORDS: *plasmonic thermal emitter, mid-infrared, Tamm plasmon, optical cavity*

The mid-infrared (mid-IR) spectral range, which contains the characteristic absorptions of organic molecules and gas molecules, is useful in a large variety of applications including biosensing[1,2] and the detection of toxic gases.[3] Conventional broadband light sources have been used in the past as mid-IR light sources; however, in recent years the need for narrowband light sources in sensing systems has generated a lot of interest in the development of narrowband emitters. For the visible range, light emitting diodes (LEDs) serve as monochromatic light sources, but LEDs cannot be extended to the IR range, as they offer limited power in the IR range.[4] As an alternative, quantum cascade lasers (QCLs) have been investigated, though their relatively high cost[5] necessitates that other low-cost emitters be developed.

One of the alternative approaches is to employ surface plasmons (SPs) to enhance the properties of thermal emitters.[6−11] Surface plasmons are coupled collective electron oscillations and electromagnetic field oscillations that can be excited at the interface between certain metals and dielectric materials.[12] The two main varieties of SPs, namely, surface plasmon polaritons (SPPs) and localized surface plasmon resonances (LSPRs), have both been applied to thermal emitters. Thermal emitters based on SPPs produce sharp emission peaks, but suffer from a strong angular dependence and a weak emittance at high temperatures as a result of the increased losses in the metal at higher temperatures decreasing the intensity and sharpness of the SPP resonance.[6,7] In contrast, thermal emitters based on LSPRs have strong but broad emission peaks.[8,9] Structures that rely on a combination of SPPs and LSPRs have been investigated to alleviate these drawbacks;[10,11] however, it has been fairly challenging for SP-based emitters to simultaneously realize thermal emission with high emittance, narrow bandwidth, and small angular and polarization dependence. Moreover, these reported SP-based emitters rely on 2D/3D patterned nanostructures,[6−11] the fabrication of which involves advanced and costly micro/nanofabrication steps.

The need for complex nanostructures to excite surface plasmon resonances is a result of the large in-plane wave vector of surface plasmon modes. Recently, a new form of plasmon that can have a zero in-plane wave vector, the Tamm plasmon (TP), has been shown to exist at the interface between a metallic mirror and distributed Bragg reflector (DBR). Having a zero in-plane wave vector means that TPs can be excited by

Received: February 20, 2018
Published: April 18, 2018

DOI: 10.1021/acsphotonics.8b00236
ACS Photonics XXXX, XXX, XXX−XXX

light propagating in free space without the need for nanostructures to couple the light.[13] Similarly, TPs excited by thermal oscillations can be out-coupled from a TP device, producing strong thermal radiation at the TP resonance wavelength, without the need for complicated nanostructures on the device.

Since the theoretical proposal of TP as a new form of SP, TPs have been implemented in a variety of devices, including photodetectors,[14,15] electrical emitters for the visible range,[16,17] and thermal emitters for the infrared range.[18,19] Having a narrow emission bandwidth in addition to being simple to fabricate makes TP structures suitable as narrowband thermal emitters. The first TP-based thermal emitter designs relied on emission through the metal film of the TP structure; however, the need for thin metal films resulted in a significant amount of absorption that decreased the emittance peak and increased the background emission, thus reducing the *Q*-factor of the devices.[18] Recently, a TP-based thermal emitter that relies on emission from the DBR side of the TP structure was demonstrated using a Si/SiO_2 DBR on a thick metal film.[19] Emission from the DBR side was found to be more efficient than emission from the metal side for mid-IR applications. A variety of devices have also been proposed and demonstrated that rely on slight modifications to the typical TP structure (consisting of a DBR and a metal layer). TP structures incorporating an optical cavity/microcavity have been used for the study of light−matter interaction,[17,20] and TP structures with a thicker DBR layer adjacent to the metal layer have also been investigated.[14,21]

In this work, we demonstrate a narrowband thermal emitter by inserting an optical cavity between a $Ge/SiO_2/Ge$ DBR and a Au film of a typical TP structure. The design relies on emission from the DBR side of this TP-cavity hybrid structure. The coupling between the cavity mode and the TP mode of the hybrid structure results in a sharper absorptance peak than achievable using a pure TP structure (without cavity). At the resonance wavelength of the coupled mode, the Au film and top DBR trap light effectively in the cavity, resulting in near unity absorptance. The electric field intensity is significantly enhanced in the optical cavity and a high *Q*-factor is achieved. In addition, the resonance wavelength of the hybrid structure can be shifted along the DBR stop band simply by varying the cavity thickness, making a wide range of emission wavelengths easily obtainable. Furthermore, the resonance wavelength of the hybrid structure shows a small polarization dependence (resonance wavelength difference between TM and TE is less than 2 nm when incident angle is lower than 30°), and a less than 20 nm shift in the absorptance peak wavelength when the incident angle is smaller than 8°. Upon thermal excitation of the hybrid structure at a temperature of 150 °C, the hybrid structure shows an emittance peak of 0.90 with a *Q*-factor as large as 88 at the same wavelength as the reflectance dip observed at room temperature. In addition, the hybrid structure has a low background emission, with the ratio between the emittance peak and the background emittance being approximately 45. The *Q*-factor and the peak to background ratio of the TP-cavity hybrid structure exceed those of many recently reported SP- or TP-based thermal emitters.[6−11,18,19] A relatively small polarization dependence as well as a low background emission render this hybrid structure superior to SPP-based thermal emitters.[6,7] The outstanding optical properties and high emittance of this easy-to-fabricate hybrid structure makes it a promising candidate for use in a variety of mid-IR applications.

As shown in the inset of Figure 1a, the hybrid structure consists of a SiO_2 optical cavity sandwiched between a Ge/SiO_2/Ge DBR structure on top and a Au film underneath. The DBR at the top of the structure is made of alternating layers of Ge and SiO_2. These two materials were chosen to provide a large refractive index contrast (n_{Ge} = 4.02 and n_{SiO2} = 1.45, at a wavelength of 5 μm), as a large index contrast results in the DBR having a spectrally wide stop band (about 6.4 μm) and a high reflectance.[22] The thickness of each DBR layer is set to make each layer having an optical thickness of one-quarter the targeted emission wavelength. On the other side of the optical cavity, a highly reflective yet slightly absorbing Au film acts as both the high-temperature source of radiation and one of the cavity mirrors (the DBR being the other). Since the structure is dedicated to mid-infrared applications, a 100 nm Au layer is

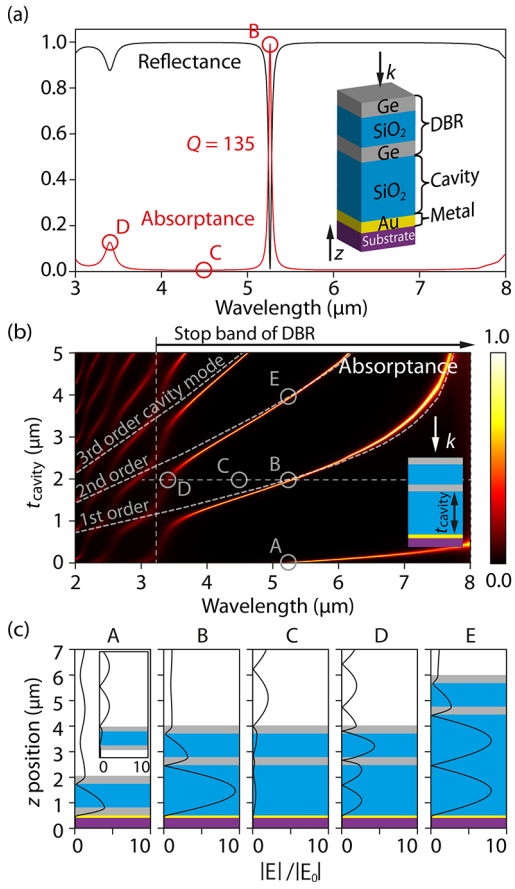

Figure 1. (a) Simulated reflectance (black solid curve) and absorptance (red solid curve) spectra for the designed hybrid structure under normal incident light, with t_{Ge} = 311 nm, t_{SiO2} = 925 nm, t_{cavity} = 1972 nm, and t_{Au} = 100 nm. The schematic diagram of the hybrid structure is shown in the inset. (b) The simulated absorptance varying with light wavelength and cavity thickness t_{cavity} under normal incident light, other layer thicknesses are kept constant and the same as in (a). The horizontal dashed line across Points B, C, and D indicates the cavity thickness used in (a), the vertical dashed line indicates the left edge of the DBR stop band, and the three dashed curves indicate different orders of cavity modes. The simulated electric field distributions of Points A (t_{cavity} = 0 nm, λ = 5.265 μm), B (t_{cavity} = 1972 nm, λ = 5.265 μm), C (t_{cavity} = 1972 nm, λ = 4.500 μm), D (t_{cavity} = 1972 nm, λ = 3.400 μm), and E (t_{cavity} = 3945 nm, λ = 5.265 μm) are shown in (c), and the inset for Point A is the electric field of a bare $Ge/SiO_2/Ge$ DBR at the same wavelength as Point A.

DOI: 10.1021/acsphotonics.8b00236
ACS Photonics XXXX, XXX, XXX−XXX

thick enough to be opaque for the range of relevant wavelengths.

The far-field reflectance and absorptance of the structure are investigated using the rigorous coupled wave analysis (RCWA) technique (DiffractMOD, Rsoft Design Group, Ossining, U.S.A.). The near-field electric field distribution is examined using the finite-difference time-domain (FDTD) technique (FullWAVE, Rsoft Design Group, Ossining, U.S.A.). The complex permittivity of Au is approximated using the Drude-Lorentz dispersion model.[23] The refractive indices of Ge and SiO_2 are modeled according to literature values.[24,25] In Figure 1a, the reflectance and absorptance spectra are shown for normal incidence with t_{Ge} = 311 nm, t_{SiO2} = 925 nm, t_{cavity} = 1972 nm, and t_{Au} = 100 nm (here t_{Ge} and t_{Au} are the thicknesses of the Ge and Au layers, respectively, t_{SiO2} is the thickness of the SiO_2 layer in the DBR, and t_{cavity} is the thickness of the SiO_2 cavity). The absorptance spectrum reveals a sharp and strong absorptance peak (corresponding to a reflectance dip). The maximum of the absorptance peak is as high as 0.993, and the absorptance peak has a Q-factor of 135. At an off resonance wavelength of 6 μm, the hybrid structure has a low absorptance of 0.002, a value which is even lower than the absorptance of a semi-infinite Au mirror (calculated to be about 0.014 at the same wavelength[23]). According to Kirchhoff's law, the emittance of a planar surface is equal to its absorptance,[26] and therefore, this structure is expected to show not only a sharp and strong emission peak, but also a low background emission.

Figure 1b shows the simulated absorptance under normal incidence as a function of wavelength λ and cavity thickness t_{cavity} (other thicknesses being kept constant). t_{cavity} = 0 (i.e., no cavity) indicates a pure TP condition, whose resonance condition can be described by[13]

$$r_{DBR}r_{Au} \sim 1 \tag{1}$$

where r_{DBR} is the reflection coefficient of a wave incident on the DBR from just after the Au layer, and r_{Au} is the reflection coefficient of the wave incident on the Au film from the DBR. For a cavity thickness of t_{cavity} = 0, a pronounced TP resonance at Point A (Figure 1b) occurs within the stop band of the DBR. To the left of Point A, there are some additional weak peaks resulting from leaky TP resonances in the side bands of the DBR (see Figure S1 in the Supporting Information).

If an optical cavity is inserted between the DBR and the Au film, the TP mode resonance condition equation must be revised to consider the phase change of the light as it propagates one round trip in the cavity. This phase change is equal to $2\pi\frac{2n_{SiO2}t_{cavity}}{\lambda}$. As a result, the resonance condition of the TP mode can be expressed as

$$r_{DBR}r_{Au}e^{i(4\pi n_{SiO2}t_{cavity})/\lambda} \sim 1 \tag{2}$$

As t_{cavity} is increased from zero, the wavelength for this new hybrid resonance condition red-shifts as can be seen to the right of Point A in Figure 1b. The phase shift induced by the cavity thickness makes it possible to select the wavelength of the resonance through changing the cavity thickness. In addition to the TP resonance of the structure, the cavity has its own resonance modes described by,

$$t_{cavity} = m\lambda/2n_{SiO2} \tag{3}$$

When the cavity thickness is increased sufficiently enough to excite one of these modes within the stop band of the DBR, a coupled TP-cavity resonance that results in strong constructive interference within the cavity and a large absorptance (Point B) is obtained. The three white dashed curves shown in Figure 1b indicate conditions for different orders of the cavity modes, as described by eq 3. It is evident from the good overlap between the strong absorptance lines and the cavity modes, as shown in Figure 1b, that the high absorptance is a result of a strongly coupled TP-cavity mode.

The near-field behavior of the hybrid structure is investigated at five points (Points A–E in Figure 1b). Points B, C, and D have the same cavity thickness as each other (t_{cavity} = 1972 nm), corresponding to the thickness used in Figure 1a; and Points A, B, and E have the same wavelength as each other. Point A, in which no SiO_2 cavity is present, represents a standard TP resonance within the stop band of the DBR. The electric field distribution at Point A, shown in Figure 1c, reveals a standing-wave pattern inside the DBR with an antinode at the upper side of the DBR and a node at the lower side. The electric field intensity has a maximum at the first Ge/SiO_2 interface and decays toward both the Au film and the Ge/air interface. In contrast to the TP resonance of Point A, a bare DBR at the same incident wavelength possesses a node at the upper side and an antinode at the lower side of the DBR, and the electric field decreases going from the upper side to the lower side, as shown in the inset for Point A in Figure 1c. The difference in phase between the bare DBR and the TP mode is related by the excitation of the TP, and allows the DBR to transmit light to the DBR/Au interface despite its normal mirror-like reflectance.

By inserting an optical cavity into the TP structure of Point A, the hybrid structure of Point B can be obtained. The strong resonance at Point B is a result of the coupling between the TP mode and the first order mode of the cavity (m = 1 in eq 3), as suggested by the similarity between the resonance dispersion and the mode dispersion (Figure 1b). The electric field distribution of Point B (Figure 1c) has, in addition to the standing-wave pattern inside the DBR typical of a TP mode, a very pronounced standing-wave pattern in the cavity. This allows energy to be trapped in the cavity, and results in a high absorptance peak Q-factor of 135 at Point B. This high Q value compares favorably with the Q = 34 obtained for the pure TP at Point A. Point C represents the properties of the background of the absorptance spectrum in Figure 1a and has a low absorptance and a high reflectance. The electric field distribution of Point C reveals the DBR behaving as a mirror (node at the top and antinode at the bottom). This means that most of the light is reflected back at the top layer of the DBR and is not absorbed in the Au. A portion of the light that is transmitted through the DBR is reflected by the bottom Au layer, and a very low intensity standing-wave between the DBR and the Au film is seen. The constructive interference between the light reflected by the different interfaces results in Point C having a reflectance larger than even an opaque Au mirror.

Points D and E both exhibit a second order standing-wave within the cavity as a result of the fact that they are both along the resonance line formed by the coupling of the second order cavity mode and the TP mode. Point D, however, has a much lower intensity, because Point D lies at the edge of the DBR stop band, where the DBR reflectance is imperfect (see Figure S1 in the Supporting Information). Here, the coupled TP-cavity mode is leaky, and as such the resonance is weak and broad. In contrast to Point D, Point E falls within the DBR stop band and the coupling condition can be fulfilled (see Figure S1). This results in Point E having a high absorptance (absorptance =

DOI: 10.1021/acsphotonics.8b00236
ACS Photonics XXXX, XXX, XXX−XXX

0.993) with a high Q-factor (Q = 211). The coupling of the TP and cavity modes is also clearly observable in Figure 1c for Point E, where a second order standing-wave pattern with a large intensity is observed. The Q-factor of the coupled mode can be increased by using higher orders of the cavity mode, but to simplify the fabrication process, the coupled mode around Point B is studied throughout the rest of this work.

It is noted that by varying the thickness of the cavity, the wavelength of the strong coupled mode can be adjusted between 4.0 and 7.5 μm, as seen in Figure 1b. Therefore, the hybrid structure makes it possible to obtain a resonance wavelength in a wide range of wavelengths simply by adjusting the optical cavity thickness. It is envisaged that electro-optical materials could be used to control the effective optical thickness of the cavity and achieve a tunable emitter.

For structures used in narrowband thermal emission, angular and polarization dependence should be characterized. The simulated absorptance spectra for different incident angles (θ) of transverse magnetic (TM-) polarized light are shown in Figure 2a. For TM-polarized incidence, resonance wavelength

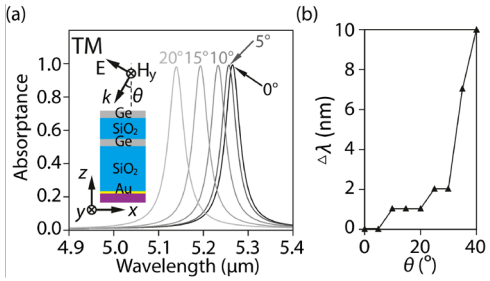

Figure 2. (a) Simulated absorptance spectra for TM-polarized light for varying incident angles (θ = 0°, 5°, 10°, 15°, and 20°) at Point B in Figure 1. (b) Difference between the center wavelength of the absorptance peaks for TM and TE polarizations as a function of θ (θ varies 5° for each point).

shifts 8 nm for θ increasing from 0° to 5°. When the incident angle changes from normal to about 8°, the absorptance shows a decrease by 50% at the wavelength of the normal incidence peak (and peak wavelength blue-shifts by 20 nm). See Figure S2 for a comparison of the angular dependence of the pure TP structure, cavity structure, and the hybrid structure. The wavelength difference ($\Delta\lambda$) between the absorptance peaks of the TM and the transverse electric (TE) polarizations for varying θ is shown in Figure 2b (see Figure S3 for TE-polarized absorptance spectra for varying θ). From this, it is clear that the absorptance peaks for TM- and TE-polarized light exhibit very little wavelength difference as θ varies from 0° to 30° (the difference is within 2 nm).

In Figure 3, the absorptance spectra of two hybrid structure designs are compared to the absorptance spectra of TP structures and Fabry–Perot cavities.[27,28] Figure 3a shows the absorptance spectra for a TP structure with a 3-layer Ge/SiO_2 DBR and a 5-layer Ge/SiO_2 layer DBR, where the high-index Ge layer is in contact with the Au film as necessary to meet the TP resonance condition.[13,19,29] The 3-layer DBR corresponds to the same hybrid structure studied in Figure 1b when t_{cavity} is zero. Point A from Figure 1b is labeled in Figure 3a. From Figure 3a, it is evident that the absorptance peak bandwidth shrinks as an addition DBR period is added; however, the intensity of the absorptance peak diminishes. The 5-layer DBR has a lower transmittance, which allows light to be effectively

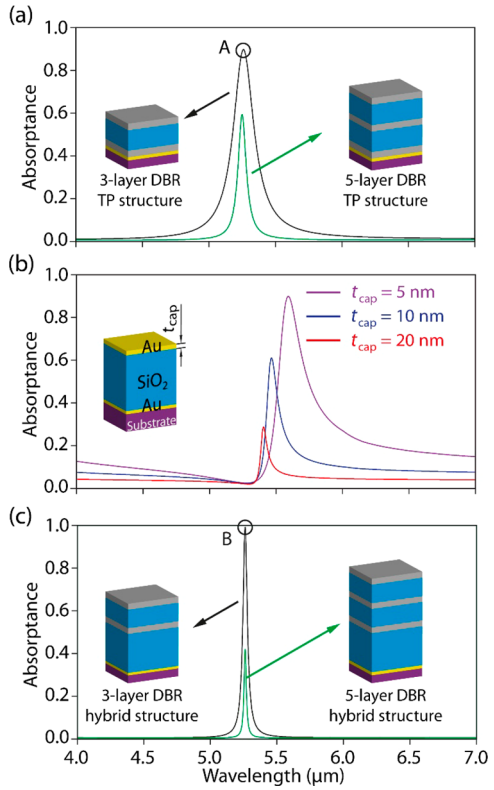

Figure 3. (a) Absorptance spectra of the 3-layer and 5-layer DBR TP structures (black and green solid curves). (b) Absorptance spectra of Au/SiO_2/Au cavity structure with different t_{cap} (thickness of surface Au). (c) Absorptance spectra of the 3-layer and 5-layer DBR hybrid structures (black and green solid curves). Points A and B are the same points as in Figure 1.

confined in the TP mode and contributes to the structure having a higher Q-factor. The reduced absorptance intensity is a result of the reduced coupling of the incident light to the TP mode at the DBR/Au-film interface. For the TP to be excited, incident light must penetrate through the DBR and reach the DBR/Au-film interface. Since the TP mode is within the stop band of the DBR, the incident light is initially reflected at the DBR/Air interface and only propagates in the DBR as an evanescently decaying wave. As the thickness of the DBR is increased by adding an additional period, the intensity of light that can reach the DBR/Au-film interface and excite the TP mode is also reduced. This results in less light being coupled from free space to the TP mode and a smaller TP absorptance peak for the structure.

Figure 3b shows the absorptance spectra for a Fabry–Perot cavity structure with different thicknesses for the top Au layer (t_{cap}). The thicknesses of the cavity and the bottom Au layer are kept constant and are t_{cavity} = 1972 nm and t_{Au} = 100 nm, respectively (the same as the hybrid structure for Point B of Figure 1b). As the top Au layer thickness is increased, the resonance bandwidth and intensity become smaller. A thicker Au top layer has a higher reflectance, which improves the light confinement and results in a higher Q-factor, but since the Au layer transmittance is lower, less light can enter the cavity and resonate, resulting in a smaller absorptance. For this reason, it is difficult to obtain a Fabry–Perot cavity that has both a large absorptance peak and a small bandwidth.

The absorptance spectra for a hybrid structure with a 3-layer DBR and a hybrid structure with a 5-layer DBR are shown in

DOI: 10.1021/acsphotonics.8b00236
ACS Photonics XXXX, XXX, XXX−XXX

Figure 3c. Both hybrid structures exhibit an absorptance spectrum similar to the TP structures, suggesting that the absorptance is related with the TP resonance; however, their absorptance peaks are narrower than both the TP structures and the Fabry–Perot structures. The coupling of the cavity and TP mode in the hybrid structure results in a more stringent excitation condition for the coupled mode, and thus, a sharper resonance. Moreover, the Q-factors of the hybrid structures are enhanced over the TP structures as a result of the cavity's ability to store a large amount of energy.

The TP-cavity hybrid structure was fabricated on a Si substrate using an RF-magnetron sputtering system (CFS-4ES, Shibaura Engineering Works Co., Ltd., Yokohama, Japan). The target dimensions of the structure were the same as the structure of Figure 1a. First, a Ti adhesion layer (10 nm thick) was deposited on the Si substrate. Subsequently, Au layer was deposited. Then, an additional Ti layer of 5 nm was sputtered on top of the Au layer. Afterward, the SiO_2 optical cavity and the Ge/SiO_2/Ge DBR structure were deposited. The dimensions of the fabricated structure were measured by scanning electron microscopy (SEM) as t_{Ge} = 298 nm, t_{SiO2} = 982 nm, t_{cavity} = 1693 nm, and t_{Au} = 106 nm, and the inset to the right of Figure 4a shows the SEM cross-section image of the fabricated structure. The reflectance spectrum of the sample was measured with plane-wave-incidence produced by FT-IR spectrometer (VIR-300, JASCO, Tokyo, Japan; see Figure S4 for detailed information about the optical setup used for reflectance measurements), and calibration was done with a Au mirror (see Figure S5). The measurements were performed with a spectral resolution of 4 cm^{-1}, which corresponds to 10 nm when the wavelength of interest is 5 μm. The measured and simulated spectra are in good agreement, as shown in Figure 4a.

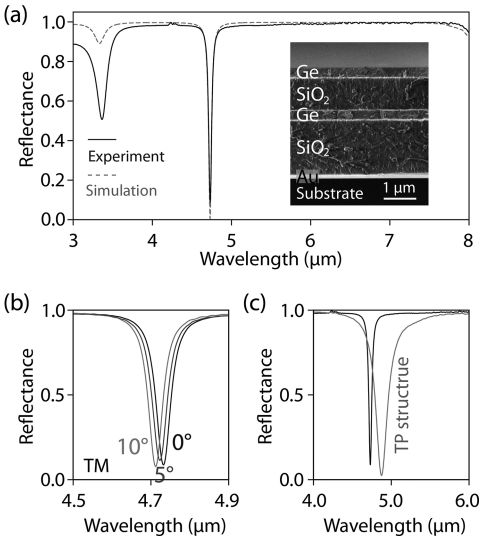

Figure 4. (a) Experimental (black solid curve) and numerical (gray dashed curve) results for the nonpolarized reflectance spectrum of the fabricated sample with t_{Ge} = 298 nm, t_{SiO2} = 982 nm, t_{cavity} = 1693 nm, t_{Au} = 106 nm, and θ = 0°. Scanning electron microscopy cross-section view of the fabricated structure is shown in the inset. (b) Measured reflectance spectra of the hybrid structure for a TM-polarized incident light with θ = 0°, 5°, and 10°. A TP structure with a Ge/SiO_2/Ge DBR (3-layer DBR TP structure) was also fabricated (t_{Ge} = 282 nm, t_{SiO2} = 886 nm, and t_{Au} = 106 nm), and a comparison between the reflectance of the TP structure (gray curve) and the hybrid structure (black solid curve) is shown in (c).

The measured reflectance spectrum shows a dip at a wavelength of 4.733 μm, with a full width at half-maximum (fwhm) of 45 nm, a Q-factor of 104 (simulated Q-factor with fabricated dimensions is 122), a dip value of 0.085, and a near unity background reflectance (0.991 at a wavelength of 6 μm). The reflectance spectra of the hybrid structure for near-normal incidence angles were measured with TM-polarized incident light. As shown in Figure 4b, the initial position of the dip at the wavelength of 4.733 μm in the reflectance spectra shifts by only 6 nm when θ is varied from 0° to 5°. The peak shifted an additional 10 nm when θ varied was further increased from 5° to 10°. In order to verify that the coupled TP-cavity mode performs better than a pure TP mode, a TP-based structure with a Ge/SiO_2/Ge DBR on an Au film was also fabricated and characterized. The dimensions of the fabricated TP structure (measured by SEM as t_{Ge} = 282 nm, t_{SiO2} = 886 nm, and t_{Au} = 106 nm) are different from those of the hybrid structure due to minor fabrication problems. The measured reflectance dip of the TP structure has a Q-factor of 27 under normal incident light (simulated Q-factor with fabricated dimensions is 28). See Figure S6 for detailed information on the TP structure. The reflectance spectra of the TP structure and the hybrid structure, as seen in Figure 4c, clearly show that the hybrid structure possesses a much narrower bandwidth than the pure TP structure.

According to Kirchhoff's law, the emittance of an object is equal to its absorptance for a given wavelength, incident angle, and polarization.[26] Based on this, a structure that has a strong and narrow absorptance peak should also have a strong and narrow emittance peak. The structure whose reflectance spectrum is shown in Figure 4a showed a strong and narrow reflectance dip, and it is expected that this peak will give rise to a narrowband and high-emittance peak in the structure's emittance spectrum. To measure the thermal emission of the TP-cavity hybrid structure, the sample was heated up to 150 °C using a heating stage (UH200CV, SPLEAD Corp., Tokyo, Japan). Emission from the sample was measured through the external port of an FT-IR spectrometer (VIR-300, JASCO, Tokyo, Japan) with a collection angle of $-8° < \theta < 8°$. A carbon soot film was deposited on a Si substrate to act as a blackbody reference. The surface temperature of the hybrid structure was measured using a K-type thermocouple equipped with a surface temperature probe (IK-500, AS ONE Corp., Osaka, Japan). The temperature of the carbon soot surface was measured using an infrared radiometer (Heitronics KT19.82, Heitronics, Wiesbaden, Germany; deviation about ±0.6 °C at 150 °C). Figure 5a shows the measured emission spectrum of the hybrid structure for a surface temperature of 150 °C, together with the emission spectrum of the carbon soot layer (blackbody reference) at the same temperature. The emittance spectrum of the tested sample can be calculated from its measured emission spectrum using a normalization procedure with the blackbody spectrum as a reference. The emittance ϵ is calculated following the approach described in the literature:[7,11,30]

$$\epsilon(\lambda, T) = \frac{E_S(\lambda, T) - E_{E1}(\lambda, T)}{E_B(\lambda, T) - E_{E2}(\lambda, T)} \quad (4)$$

where E_B is the estimated emission of a perfect blackbody, E_S is the measured sample emission, E_{E1} is the environmental emission of the sample, E_{E2} is the environmental emissions of the blackbody, and T is the surface temperature used.

DOI: 10.1021/acsphotonics.8b00236
ACS Photonics XXXX, XXX, XXX−XXX

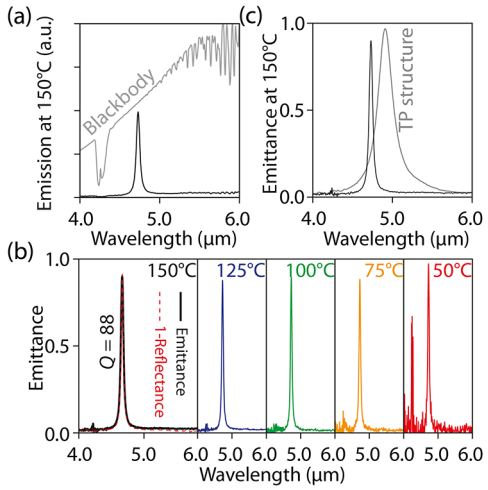

Figure 5. (a) Emission spectrum of the hybrid structure for a surface temperature of 150 °C (black), and the emission spectrum of the blackbody reference at the same temperature (gray). Dips seen in the blackbody emission spectrum at around 4.25 and 6.00 μm are due to absorption by ambient CO_2 and H_2O, respectively. (b) Calculated emittance spectra of the fabricated sample at different temperatures. The absorptance (1 - reflectance) spectrum (red dashed curve) of the structure at 150 °C is shown as a reference. (c) Comparison between the emittance of the TP structure (gray solid curve) and the hybrid structure (black solid curve).

Emittance spectra of the hybrid structure at different surface temperatures (50, 75, 100, 125, and 150 °C) are shown in Figure 5b. The absorptance spectrum for the sample at room temperature, (1 - reflectance), is also shown for comparison. The calculated emittance of the sample for a temperature of 150 °C reaches up to 0.90 at 4.731 μm, with a *Q*-factor as high as 88 and a low background emittance (about 0.02 at wavelength of 6 μm) in the vicinity of the emittance peak. The ratio between the emittance peak and the background emittance (about 45), and the *Q*-factor of this structure are larger than any other values reported for SP-based thermal emitters,[6−11,18,19] including TP-based thermal emitters.[18,19] The peak in the emittance spectrum is found to be slightly weaker and broader than the observed absorptance peak at room temperature, and the background of the emittance spectrum is found to be slightly stronger than the observed absorptance spectrum. These slight deviations from the observed absorptance are attributed to the averaging of the emittance spectrum over the FT-IR collection angle (±8°) and to the increased loss factor of the Au and SiO_2 layer at elevated temperatures. As the surface temperature decreases from 150 to 75 °C, the maximum emittance remains relatively constant, ranging from 0.88 to 0.90; the *Q*-factor slightly increases from 87.5 to 88.3; and the emittance peak blue-shifts by 7 nm. These small changes in the emittance peaks are likely caused by thermal expansion of the layers and/or variations in the optical properties with temperature. At a low temperature of 50 °C, due to the weak intensity of thermal emission (proportional to T^4), noise in the measurement, especially around the CO_2 absorption window (about 4.25 μm), becomes significant in comparison to the emission intensity. The pure TP structure exhibits an emittance peak (with a *Q*-factor of 22) broader than the hybrid structure at 150 °C, as shown in Figure 5(c). In summary, by inserting a cavity between the DBR and the Au film of a standard TP structure, a hybrid structure sustaining a coupled TP-cavity mode that has a low background emission and a high *Q*-factor was obtained.

A hybrid TP-cavity structure consisting of an optical cavity sandwiched between a DBR and a Au film was proposed as a narrowband and high-emittance thermal emitter. Through studying the near-field and far-field behaviors of the hybrid structure, it was found that the coupling of the TP mode of the Au film and DBR, and the cavity modes of the optical cavity results in the hybrid structure having a sharp and large reflectance dip in the mid-IR. The fabricated hybrid structure was found to have a strong mid-IR emittance (0.90 at 4.731 μm), with a high *Q*-factor (*Q* = 88) and a low background emittance (0.02), when heated to 150 °C. This performance exceeds the performance of similar TP-based emitters and demonstrates the potential of the hybrid TP-cavity structure. The incorporation of tunable optical cavities in the future may pave the way for high-performance, narrowband and tunable mid-IR thermal emitters.

■ ASSOCIATED CONTENT

Supporting Information

The Supporting Information is available free of charge on the ACS Publications website at DOI: 10.1021/acsphotonics.8b00236.

Calculated amplitude of propagating wave and its phase difference after a round trip in the cavity, simulated dispersion diagrams of absorptance for the pure TP, the cavity, and the hybrid structures, simulated angular dependence information for the hybrid structure with TM and TE polarizations, schematic diagram of reflectance measurement setup, calibration process of measured reflectance, and measurement of the reflectance and emission spectra of the TP structure (PDF).

■ AUTHOR INFORMATION

Corresponding Author

*E-mail: jean@mech.t.u-tokyo.ac.jp.

ORCID

Zhiyu Wang: 0000-0002-6614-1661
Ya-Lun Ho: 0000-0001-8274-5978
Hirofumi Daiguji: 0000-0001-6896-3282
Jean-Jacques Delaunay: 0000-0003-2175-0620

Funding

This work was supported through Japan Society for the Promotion of Science (JSPS) KAKENHI Grant Numbers (17K18867, 17H03229), and JSPS Core-to-Core Program (Advanced Research Networks type A), Japan.

Notes

The authors declare no competing financial interest.

■ ACKNOWLEDGMENTS

This work was supported through Japan Society for the Promotion of Science (JSPS) KAKENHI Grant Numbers (17K18867, 17H03229) and JSPS Core-to-Core Program (Advanced Research Networks type A), Japan. A part of this work was conducted in the Center for Nano Lithography and Analysis, The University of Tokyo, supported by the Ministry of Education, Culture, Sports, Science and Technology (MEXT), Japan. We would like to extend our grateful appreciation to Ms. Ayako Mizushima and Dr. Eric Lebrasseur from The University of Tokyo for important technical support.

DOI: 10.1021/acsphotonics.8b00236
ACS Photonics XXXX, XXX, XXX−XXX

REFERENCES

(1) Lin-Vien, D.; Colthurp, N. B.; Fateley, W. G.; Grasselli, J. G. *The Handbook of Infrared and Raman Characteristic Frequencies of Organic Molecules*; Academic Press, 1991.

(2) Kaplan, H. *Practical Applications of Infrared Thermal Sensing and Imaging Equipment*; SPIE Press, 2007.

(3) Chen, W.; Mouret, G.; Boucher, D.; Tittel, F. K. Mid-infrared trace gas detection using continuous-wave difference frequency generation in periodically poled $RbTiOAsO_4$. *Appl. Phys. B: Lasers Opt.* **2001**, *72*, 873−876.

(4) Schubert, E. F. *Light-Emitting Diodes*; Cambridge University Press, 2006.

(5) Yao, Y.; Hoffman, A. J.; Gmachl, C. F. Mid-infrared quantum cascade lasers. *Nat. Photonics* **2012**, *6*, 432.

(6) Chen, C.-Y.; Tsai, M.-W.; Jiang, Y.-W.; Ye, Y.-H.; Chang, Y.-T.; Lee, S.-C. Coupling of surface plasmons between two silver films in a plasmonic thermal emitter. *Appl. Phys. Lett.* **2007**, *91*, 243111.

(7) Liu, J.; Guler, U.; Lagutchev, A.; Kildishev, A.; Malis, O.; Boltasseva, A.; Shalaev, V. M. Quasi-coherent thermal emitter based on refractory plasmonic materials. *Opt. Mater. Express* **2015**, *5*, 2721−2728.

(8) Liu, X.; Tyler, T.; Starr, T.; Starr, A. F.; Jokerst, N. M.; Padilla, W. J. Taming the blackbody with infrared metamaterials as selective thermal emitters. *Phys. Rev. Lett.* **2011**, *107*, 045901.

(9) Lochbaum, A.; Fedoryshyn, Y.; Dorodnyy, A.; Koch, U.; Hafner, C.; Leuthold, J. On-chip narrowband thermal emitter for mid-IR optical gas sensing. *ACS Photonics* **2017**, *4*, 1371−1380.

(10) Miyazaki, H. T.; Ikeda, K.; Kasaya, T.; Yamamoto, K.; Inoue, Y.; Fujimura, K.; Kanakugi, T.; Okada, M.; Hatade, K.; Kitagawa, S. Thermal emission of two-color polarized infrared waves from integrated plasmon cavities. *Appl. Phys. Lett.* **2008**, *92*, 141114.

(11) Wang, Z.; Clark, J. K.; Huang, L.-C.; Ho, Y.-L.; Delaunay, J.-J. Plasmonic nanochannel structure for narrow-band selective thermal emitter. *Appl. Phys. Lett.* **2017**, *110*, 251102.

(12) Schuller, J. A.; Barnard, E. S.; Cai, W.; Jun, Y. C.; White, J. S.; Brongersma, M. L. Plasmonics for extreme light concentration and manipulation. *Nat. Mater.* **2010**, *9*, 193.

(13) Kaliteevski, M.; Iorsh, I.; Brand, S.; Abram, R. A.; Chamberlain, J. M.; Kavokin, A. V.; Shelykh, I. A. Tamm plasmon-polaritons: Possible electromagnetic states at the interface of a metal and a dielectric Bragg mirror. *Phys. Rev. B: Condens. Matter Mater. Phys.* **2007**, *76*, 165415.

(14) Zhang, C.; Wu, K.; Giannini, V.; Li, X. Planar hot-electron photodetection with tamm plasmons. *ACS Nano* **2017**, *11*, 1719−1727.

(15) Li, R.; Zhang, C.; Li, X. Schottky hot-electron photodetector by cavity-enhanced optical Tamm resonance. *Appl. Phys. Lett.* **2017**, *110*, 013902.

(16) Zhang, X. L.; Feng, J.; Han, X. C.; Liu, Y. F.; Chen, Q. D.; Song, J. F.; Sun, H. B. Hybrid Tamm plasmon-polariton/microcavity modes for white top-emitting organic light-emitting devices. *Optica* **2015**, *2*, 579−584.

(17) Brückner, R.; Zakhidov, A. A.; Scholz, R.; Sudzius, M.; Hintschich, S.; Fröb, H.; Lyssenko, V.; Leo, K. Phase-locked coherent modes in a patterned metal-organic microcavity. *Nat. Photonics* **2012**, *6*, 322−326.

(18) Yang, Z.-Y.; Ishii, S.; Yokoyama, T.; Dao, T. D.; Sun, M.-G.; Nagao, T.; Chen, K.-P. Tamm plasmon selective thermal emitters. *Opt. Lett.* **2016**, *41*, 4453−4456.

(19) Yang, Z.-Y.; Ishii, S.; Yokoyama, T.; Dao, T. D.; Sun, M.-G.; Pankin, P. S.; Timofeev, I. V.; Nagao, T.; Chen, K.-P. Narrowband wavelength selective thermal emitters by confined tamm plasmon polaritons. *ACS Photonics* **2017**, *4*, 2212−2219.

(20) Lundt, N.; Klembt, S.; Cherotchenko, E.; Betzold, S.; Iff, O.; Nalitov, A. V.; Klaas, M.; Dietrich, C. P.; Kavokin, A. V.; Höfling, S.; Schneider, C. Room-temperature Tamm-plasmon exciton-polaritons with a WSe 2 monolayer. *Nat. Commun.* **2016**, *7*, 13328.

(21) Zhou, H.; Yang, G.; Wang, K.; Long, H.; Lu, P. Multiple optical Tamm states at a metal−dielectric mirror interface. *Opt. Lett.* **2010**, *35*, 4112−4114.

(22) Joannopoulos, J. D.; Johnson, S. G.; Winn, J. N.; Meade, R. D. *Photonic Crystals: Molding the Flow of Light*, 2nd ed.; Princeton University Press, 2008.

(23) Rakić, A. D.; Djurišić, A. B.; Elazar, J. M.; Majewski, M. L. Optical properties of metallic films for vertical-cavity optoelectronic devices. *Appl. Opt.* **1998**, *37*, 5271−5283.

(24) Palik, E. D., Ed. In *Handbook of Optical Constants of Solids*; Academic Press, 1998; Vol. 3.

(25) Kischkat, J.; Peters, S.; Gruska, B.; Semtsiv, M.; Chashnikova, M.; Klinkmüller, M.; Fedosenko, O.; Machulik, S.; Aleksandrova, A.; Monastyrskyi, G.; Flores, Y.; Masselink, W. T. Mid-infrared optical properties of thin films of aluminum oxide, titanium dioxide, silicon dioxide, aluminum nitride, and silicon nitride. *Appl. Opt.* **2012**, *51*, 6789−6798.

(26) Siegel, R.; Howell, J. *Thermal Radiation Heat Transfer*; Taylor & Francis: New York, 2002.

(27) Wang, L. P.; Lee, B. J.; Wang, X. J.; Zhang, Z. M. Spatial and temporal coherence of thermal radiation in asymmetric Fabry-Perot resonance cavities. *Int. J. Heat Mass Transfer* **2009**, *52*, 3024−3031.

(28) Wang, L. P.; Basu, S.; Zhang, Z. M. Direct measurement of thermal emission from a Fabry−Perot cavity resonator. *J. Heat Transfer* **2012**, *134*, 072701.

(29) Kaliteevski, M.; Brand, S.; Abram, R. A.; Iorsh, I.; Kavokin, A. V.; Shelykh, I. A. Hybrid states of Tamm plasmons and exciton polaritons. *Appl. Phys. Lett.* **2009**, *95*, 251108.

(30) Marquier, F.; Joulain, K.; Mulet, J.-P.; Carminati, R.; Greffet, J.-J.; Chen, Y. Coherent spontaneous emission of light by thermal sources. *Phys. Rev. B: Condens. Matter Mater. Phys.* **2004**, *69*, 155412.

DOI: 10.1021/acsphotonics.8b00236
ACS Photonics XXXX, XXX, XXX−XXX